Electronic Supporting Information (ESI)

Solution-processable Benzothiadiazole/triphenylamine-based hybridized local and charge-transfer (HLCT) hyper-structured molecular red emitter for OLEDs

Xiaoyu Yin[a], Junrong Pu[b], Chen Ma[a], Yi Wu[a], Kunlun Wang[a], Yingliang Liu[a], Shaokui Cao[a], Shi-Jian Su[b,*], Shengang Xu[a,*]

* Corresponding author.

E-mail addresses: xusg@zzu.edu.cn (S. Xu), mssjsu@scut.edu.cn (S. Su).

Table of contents:

1 Instrumentation

^{1}H NMR spectra were taken on Bruker DPX-600 and Bruker DPX-400 Spectrometer at room temperature. Chemical shift values are reported in parts per million (ppm) relative to tetramethylsilane (TMS) (0 ppm) as an internal standard. Fourier transform infrared spectra (FT-IR) spectra were acquired using a Nicolet Is-10 spectrometer over the wavenumber range of 500-4000 cm^{-1} on KBr pellets. Mass spectra were determined by a Bruker Autoflex Speed MALDA-TOF in the linear mode, and trans-2-[3-(4-tert-Butylphenyl)-2-methyl-2-propenylidene] malononitrile was used as the matrix. Thermal properties were determined by thermogravimetric analysis (TGA) using a Mettler Toledo TGA/DSC simultaneous thermal analyzer at a heating rate of 10 ℃ min^{-1} under nitrogen. Differential scanning calorimetry (DSC) was performed on a NETZSCH STA449F3 Jupiter differential scanning calorimeter at a heating rate of 10 ℃ min^{-1} from 20 to 250 ℃ under nitrogen. All DSC data were collected from the second cycle of the DSC curve. The X-ray diffraction (XRD) patterns were performed on a Bruker AXS D8 Advance diffractometer with Cu Kα radiation. UV-Vis absorption spectra were recorded on an Agilent Cary 5000 UV-Vis-NIR spectrophotometer. Photoluminescence (PL) spectra were obtained using a photoluminescence spectrometer (Horiba Jobin Yvon, FluoroMax-4). Cyclic voltammetry (CV) studies were conducted using a CHI 660E voltammetry analyzer in a typical three-electrode cell with a platinum sheet working electrode, a platinum wire counter electrode, and a silver/silver nitrate (Ag/Ag+) reference electrode. The oxidation and reduction potentials were measured in acetonitrile solution with 0.1 M of tetrabutylammonium perchlorate as a supporting electrolyte at a scan rate of 0.05 V/s. Transient PL decay spectra were conducted on FLS980 (Edinburgh Instrument), the delayed spectra were measured in FLS980 utilizing a time-gated controller.

2 Synthesis

2.1 Synthesis of mCP-N_3

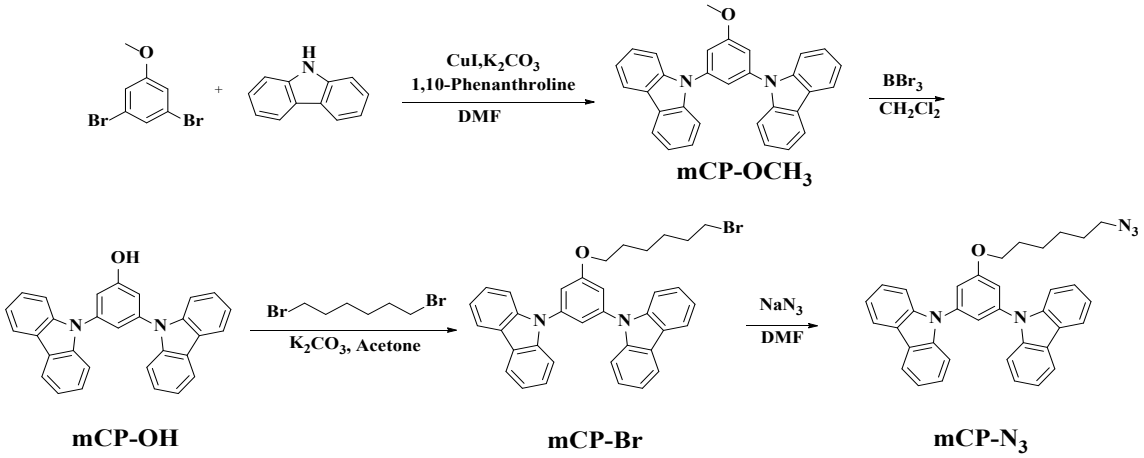

Scheme S1. Synthetic routes of mCP-N_3.

2.2 Synthesis of CRA-Alkyne

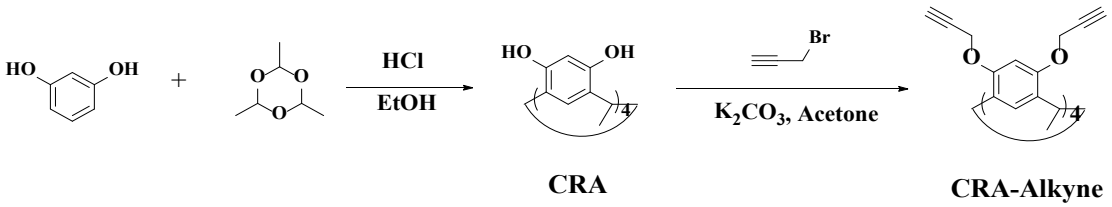

Scheme S2. Synthetic routes of CRA-Alkyne.

CRA-Alkyne was synthesized and structurally confirmed based on our previous work[1] and mCP-N_3 was synthesized according to the literature method[2-4].

2.3 Synthesis of MTBP-N_3

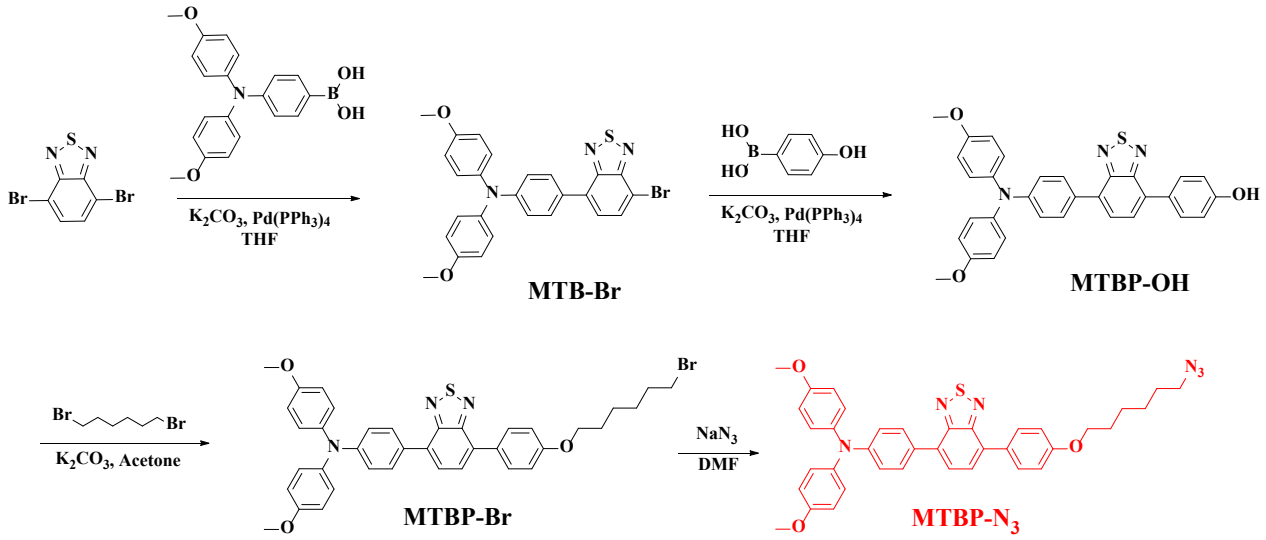

Scheme S3. Synthetic routes of MTBP-N_3.

MTB-Br: 4,7-dibromo-2,1,3-benzothiadiazole (2.65 g, 9.0 mmol) and (4-(bis(4-methoxyphenyl)amino)phenyl)boronic acid (2.10 g, 6.0 mmol) were dissolved in THF (40 mL), and 18 mL of K_2CO_3 (2.0 M aqueous solution) was added to the mixture, then the catalytic amount of $Pd(PPh_3)_4$ was added to the mixture in nitrogen atmosphere. The mixture was heated to 80 ℃ and stirred for 8 h. After the reaction was completed, the mixture was cooled to room temperature, extracted with dichloromethane, washed with deionized water, dried with anhydrous $MgSO_4$, filtered and concentrated. The crude product was purified by silica gel column chromatography with dichloromethane/petroleum ether (1/5, v/v) as eluent. A red solid powder was obtained with a yield of 70.1% (2.18 g). ^{1}H NMR (400 MHz, $CDCl_3$) δ 7.90 (d, J = 7.7 Hz, 1H), 7.80 – 7.73 (m, 2H), 7.53 (d, J = 7.6 Hz, 1H), 7.18 – 6.86 (m, 10H), 3.84 (s, 6H).

MTBP-OH: MTB-Br (1.97 g, 3.8 mmol) and (4-hydroxyphenyl)boronic acid (786.2 mg, 5.7 mmol) were dissolved in THF (40 mL), and 14 mL of K_2CO_3 (2.0 M aqueous solution) was added to the mixture, then the catalytic amount of $Pd(PPh_3)_4$ was added to the mixture in nitrogen atmosphere. The mixture was heated to 80 ℃ and stirred for 15 h. After the reaction was completed, the mixture was cooled to room temperature, extracted with dichloromethane, washed with deionized water, dried with anhydrous $MgSO_4$, filtered and concentrated. The crude product was purified by silica gel column chromatography with ethyl acetate/petroleum ether (1/5, v/v) as eluent. A red solid powder was obtained with a yield of 83.7% (1.69 g).^{1}H NMR (400 MHz, DMSO-d_6) δ 9.74 (s, 1H), 7.91 – 7.77 (m, 6H), 7.14 – 7.07 (m, 4H), 6.98 – 6.87 (m, 8H), 3.76 (s, 6H).

MTBP-Br: MTBP-OH (1.49 g, 2.8 mmol) and 1,6-dibromohexane (1.55 g, 11.2 mmol) were dissolved in acetone (50 mL), and anhydrous K_2CO_3 (1.55 g, 11.2 mmol) was added. The mixture was heated to 60 ℃ and stirred

for 12 h. After the reaction was completed, the mixture was cooled to room temperature, extracted with dichloromethane, washed with deionized water, dried with anhydrous $MgSO_4$, filtered and concentrated. The crude product was purified by silica gel column chromatography with dichloromethane/petroleum ether (1/3, v/v) as eluent. A red solid powder was obtained with a yield of 91.4 % (1.78 g). ^{1}H NMR (400 MHz, $CDCl_3$) δ 7.97 – 7.71 (m, 6H), 7.24 – 6.84 (m, 12H), 4.08 (t, J = 6.4 Hz, 2H), 3.84 (s, 6H), 3.47 (t, J = 6.7 Hz, 2H), 1.91 (dt, J = 27.3, 6.9 Hz, 4H), 1.60 – 1.55 (m, 4H).

MTBP-N_3: MTBP-Br (1.39 g, 2.0 mmol) was dissolved in DMF (30 mL) and sodium azide (520.1 mg, 8.0 mmol) was added in a nitrogen atmosphere. The mixture was heated to 60 ℃ and stirred for 12 h. After the reaction was completed, the mixture was cooled to room temperature, extracted with dichloromethane, washed with saturated NaCl solution, dried with anhydrous $MgSO_4$, filtered and concentrated. The crude product was purified by silica gel column chromatography with dichloromethane/petroleum ether (1/3, v/v) as eluent. A red solid powder was obtained with the yield of 93.5 % (1.23 g).^{1}H NMR (400 MHz, $CDCl_3$) δ 7.97 – 7.71 (m, 6H), 7.24 – 6.84 (m, 12H), 4.08 (t, J = 6.4 Hz, 2H), 3.84 (s, 6H), 3.47 (t, J = 6.7 Hz, 2H), 1.91 (dt, J = 27.3, 6.9 Hz, 4H), 1.60 – 1.55 (m, 4H). FT-IR (KBr), *v* (cm^{-1}):2936 cm^{-1}, 2864 cm^{-1} (-C-H), 2090 cm^{-1} (-N_3), 1487 cm^{-1} (-C=N-, benzothiazole). HR-MS (EI) *m/z*: [M+H]$^+$ calcd for $C_{38}H_{36}N_6O_3S$ 656.2631; found, 657.2644.

2.4 Synthesis of CRA-MTBP$_{(X)}$-mCP$_{(8-X)}$ (X=8, 7, 6, 4, 2, 1 or 0)

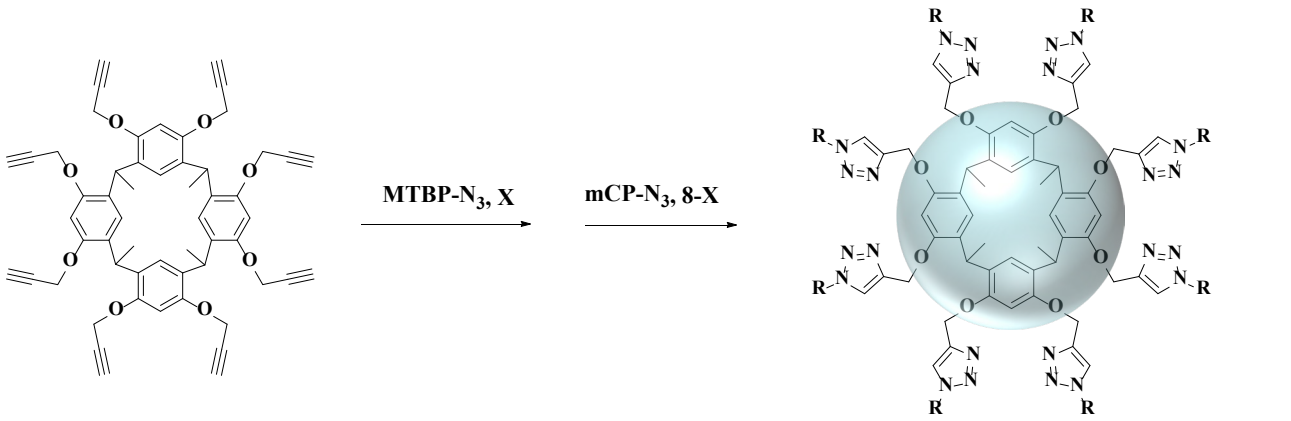

CRA-Alkyne **CRA-MTBP$_{(X)}$-mCP$_{(8-X)}$ (X= 8, 7, 6, 4, 2, 1 or 0)**

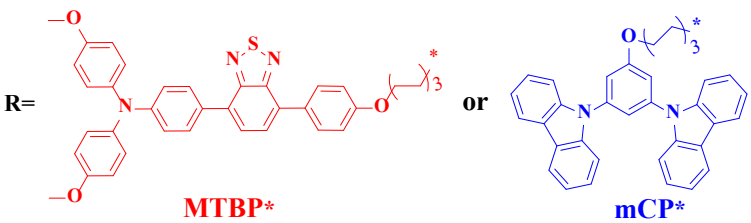

Scheme S4. Synthetic routes of CRA-MTBP$_{(X)}$-mCP$_{(8-X)}$ (X=8, 7, 6, 4, 2, 1 or 0)

General synthesis of HSMs using CRA- MTBP$_{(7)}$-mCP$_{(1)}$ as an example. CRA-Alkyne (34.0 mg, 0.04 mmol including 0.32 mmol alkynyl group) and MTBP-N_3 (184.2 mg, 0.28 mmol) were added into a Schlenk tube (20 mL), then PMDETA (124 μL, 0.08 mmol) and CuBr (57.8 mg, 0.40 mmol) were added under nitrogen atmosphere, respectively, and then the purified THF (10 mL) was added. The mixture was heated to 60 ℃ and stirred for 8 h without light. Subsequently, mCP-N_3 (65.9 mg, 0.12 mmol) was added to the mixture under a nitrogen atmosphere. The mixture was heated to 60 ℃ and stirred for other 16 h without light. After that, the rection mixture was exposed to air and stirred for 2h, then 1,4,7,10-tetraazacyclododecane (173.5 mg, 1.00 mmol) was added and stirred for 2 h. The reaction mixture was filtered through celite, extracted with dichloromethane, transferred to a separatory funnel, washed with deionized water, dried with anhydrous $MgSO_4$, filtered, and concentrated. The crude product was purified by silica gel column chromatography. The crude product was purified by silica gel column chromatography using ethyl acetate/dichloromethane (1/1, v/v) as eluent Then the obtained product was purified by Soxhlet extraction with methanol for 3 days. A red solid powder was obtained with a yield of 67.4 % (139.4 mg). ^{1}H NMR (400 MHz, $CDCl_3$) δ 7.86 (d, J = 8.2 Hz, 1H), 7.79 (d, J = 8.0 Hz, 2H), 7.59 (dd, J = 28.9, 12.0 Hz, 2H), 7.28 (s, 1H), 7.14 (d, J = 8.8 Hz, 3H), 7.02 (dd, J = 25.9, 8.5 Hz, 4H), 6.91-6.82 (m, 3H), 5.19 (d, J = 13.9 Hz, 1H), 4.40 (s, 1H), 4.31 (s, 1H), 3.97 (s, 2H), 3.82 (s, 4H), 1.98 (s, 1H), 1.91 (s, 1H), 1.53 (s, 1H), 1.44 (s, 3H), 1.43 (s, 0H). FT-IR (KBr), ν (cm^{-1}): 2864 (-C-H), 1487 cm^{-1} (-C=N-, benzothiazole). MALDI-TOF MS m/z: $[M+H]^+$ calcd for $C_{358}H_{331}N_{47}O_{30}S_7$ 5992.3946; found, 6006.2631.

CRA-MTBP$_{(8)}$-mCP$_{(0)}$. The synthetic method of CRA-MTBP$_{(8)}$-mCP$_{(0)}$ was the same as CRA-MTBP$_{(7)}$-mCP$_{(1)}$ but only MTBP-N_3 (262.7 mg, 0.40 mmol) was used for 16 h to obtain a red solid (231.52 mg, 93.1%). ^{1}H NMR (400 MHz, $CDCl_3$) δ 7.86 (d, J = 8.2 Hz, 2H), 7.79 (d, J = 8.4 Hz, 3H), 7.63 (d, J = 15.8 Hz, 2H), 7.48 (s, 0H), 7.14 (d, J = 8.5 Hz, 5H), 7.02 (dd, J = 25.2, 8.4 Hz, 5H), 6.91-6.83 (m, 4H), 5.19 (d, J = 12.2 Hz, 1H), 4.82 (d, J = 11.2 Hz, 1H), 4.41 (s, 1H), 4.32 (s, 1H), 3.98 (d, J = 6.8 Hz, 2H), 3.82 (s, 5H), 2.42 (s, 1H), 2.25 (s, 1H), 1.99 (s, 1H), 1.91 (s, 1H), 1.79 (t, J = 7.4 Hz, 2H), 1.44 (d, J = 7.4 Hz, 3H). FT-IR (KBr), ν (cm^{-1}): 2864 (-C-H), 1487 cm^{-1} (-C=N-, benzothiazole). MALDI-TOF MS m/z: $[M+H]^+$ calcd for $C_{360}H_{336}N_{48}O_{32}S_8$ 6099.3987; found, 6099.6352.

CRA-MTBP$_{(6)}$-mCP$_{(2)}$. MTBP-N_3 (158.3 mg, 0.24 mmol) and mCP-N_3 (87.9 mg, 0.16 mmol) were used to obtain a red solid (200.4 mg, 85.5%). ^{1}H NMR (400 MHz, $CDCl_3$) δ 8.13 (d, J = 7.8 Hz, 1H), 7.86 (d, J = 8.1 Hz, 1H), 7.79 (d, J = 8.0 Hz, 2H), 7.65 (s, 1H), 7.62-7.52 (m, 1H), 7.41 (t, J = 7.6 Hz, 1H), 7.28 (s, 1H), 7.14 (d, J = 8.1 Hz, 3H), 7.09-7.00 (m, 2H), 6.98 (s, 1H), 6.91-6.83 (m, 3H), 5.17 (s, 1H), 4.80 (s, 0H), 4.40 (s, 1H), 4.30 (s, 2H), 3.97 (s, 2H), 3.82 (s, 4H), 1.98 (s, 1H), 1.90 (s, 1H), 1.78 (s, 2H), 1.46 (s, 1H), 1.43 (s, 5H). FT-IR (KBr), ν (cm^{-1}):

2864 (-C-H), 1487 cm^{-1} (-C=N-, benzothiazole).

CRA-MTBP$_{(4)}$-mCP$_{(4)}$. MTBP-N_3 (105.1 mg, 0.16 mmol) and mCP-N_3 (131.9 mg, 0.24 mmol) were used to obtain a red solid (160.9 mg, 73.1%). ^{1}H NMR (400 MHz, $CDCl_3$) δ 8.12 (s, 1H), 7.85 (s, 1H), 7.80 (s, 1H), 7.64 (s, 1H), 7.55 (d, J = 8.3 Hz, 2H), 7.42 (s, 1H), 7.21- 7.11 (m, 2H), 7.05 (d, J = 8.1 Hz, 1H), 6.98 (s, 1H), 6.91-6.83 (m, 2H), 5.16 (s, 1H), 4.64 (s, 1H), 4.30 (s, 1H), 3.97 (s, 2H), 3.82 (d, J = 1.7 Hz, 2H), 2.15 (s, 0H), 1.89 (s, 2H), 1.78 (s, 1H). FT-IR (KBr), *v* (cm^{-1}): 2864 (-C-H), 1487 cm^{-1} (-C=N-, benzothiazole).

CRA-MTBP$_{(2)}$-mCP$_{(6)}$. MTBP-N_3 (53.1 mg, 0.08 mmol) and mCP-N_3 (175.9 mg, 0.32 mmol) were used to obtain a red solid (137.2 mg, 66.6%). ^{1}H NMR (400 MHz, $CDCl_3$) δ 8.12 (s, 2H), 7.80 (s, 1H), 7.56 (dt, J = 6.4, 3.1 Hz, 2H), 7.42 (d, J = 8.6 Hz, 2H), 7.28 (s, 0H), 7.21 – 7.11 (m, 2H), 7.02 (dd, J = 27.0, 9.0 Hz, 1H), 6.92 – 6.84 (m, 1H), 5.11 (s, 1H), 4.26 (s, 2H), 3.97 (s, 2H), 3.83 (d, J = 1.7 Hz, 1H), 1.86 (s, 3H), 1.43 (s, 4H). FT-IR (KBr), *v* (cm^{-1}): 2864 (-C-H), 1487 cm^{-1} (-C=N-, benzothiazole).

CRA-MTBP$_{(1)}$-mCP$_{(7)}$. MTBP-N_3 (23.9 mg, 0.04 mmol) and mCP-N_3 (197.9 mg, 0.36 mmol) were used to obtain a red solid (121.8 mg, 61.2%). ^{1}H NMR (400 MHz, $CDCl_3$) δ 8.11 (s, 2H), 7.56 (d, J = 8.4 Hz, 2H), 7.41 (s, 3H), 7.28 (s, 2H), 7.17 (s, 2H), 7.20 – 7.12 (m, 0H), 5.09 (s, 1H), 4.35 (s, 1H), 4.23 (s, 1H), 3.96 (s, 2H), 3.83 (s, 1H), 1.77 (s, 3H), 1.36 (s, 4H). FT-IR (KBr), *v* (cm^{-1}): 2864 (-C-H), 1487 cm^{-1} (-C=N-, benzothiazole).

CRA-MTBP$_{(0)}$-mCP$_{(8)}$. mCP-N_3 (219.9 mg, 0.40 mmol) was used for 16 h to obtain a white solid (140.7 mg, 73.3%). ^{1}H NMR (400 MHz, $CDCl_3$) δ 8.11 (s, 6H), 7.57 (dd, J = 17.0, 8.1 Hz, 5H), 7.28 (s, 2H), 7.16 (s, 2H), 5.32 (s, 1H), 5.08 (s, 1H), 4.33 (s, 0H), 4.22 (s, 2H), 4.05 (s, 0H), 3.96 (s, 2H), 1.84 (s, 3H), 1.47 (s, 3H), 1.39 (d, J = 7.2 Hz, 1H), 1.33 (s, 3H). FT-IR (KBr), *v* (cm^{-1}): 2864 (-C-H), 1487 cm^{-1} (-C=N-, benzothiazole).

3 ^{1}H NMR spectra

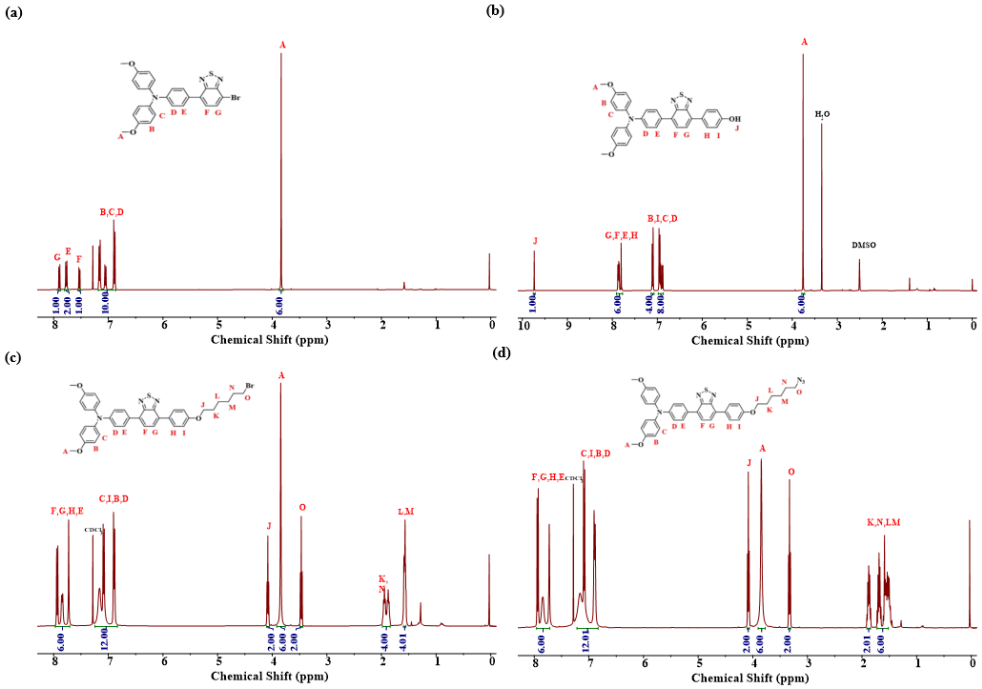

Fig. S1. ^{1}H NMR spectra of (a) MTB-Br; (c) MTBP-Br and (d) MTBP-N_3 in $CDCl_3$; (b) MTBP-OH in DMSO-d_6.

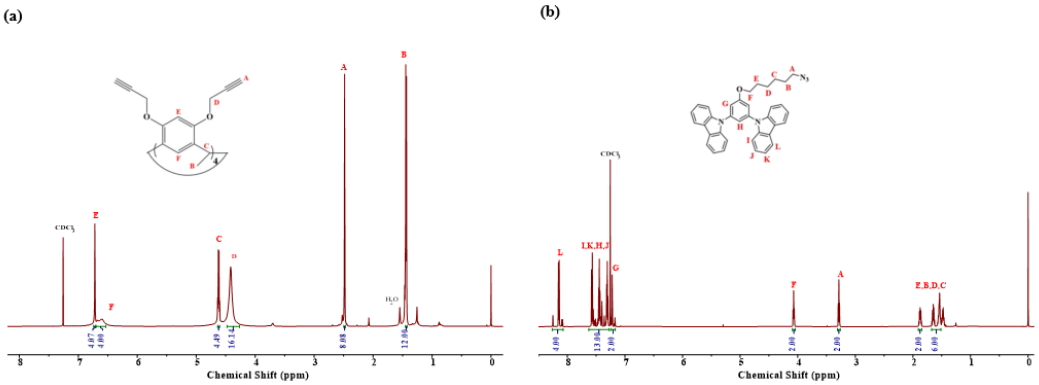

Fig. S2. ^{1}H NMR spectra of (a) CRA-Alkyne and (b) mCP-N_3 in $CDCl_3$.

4 MALDI-TOF MS spectra

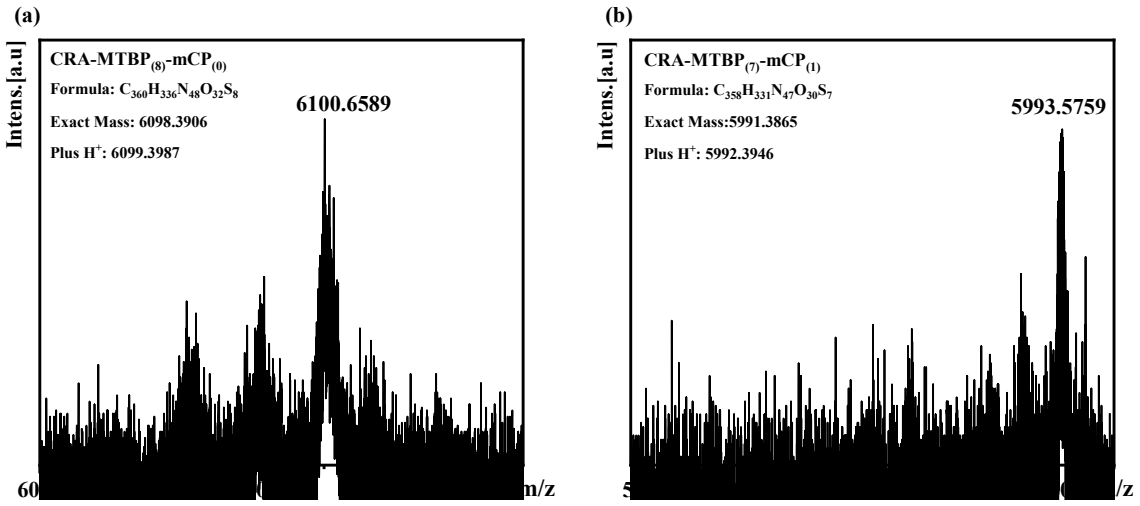

Fig. S3. MALDI-TOF MS spectra of (a) CRA-MTBP$_{(8)}$-mCP$_{(0)}$ and CRA-MTBP$_{(7)}$-mCP$_{(1)}$.

5 FT-IR spectra

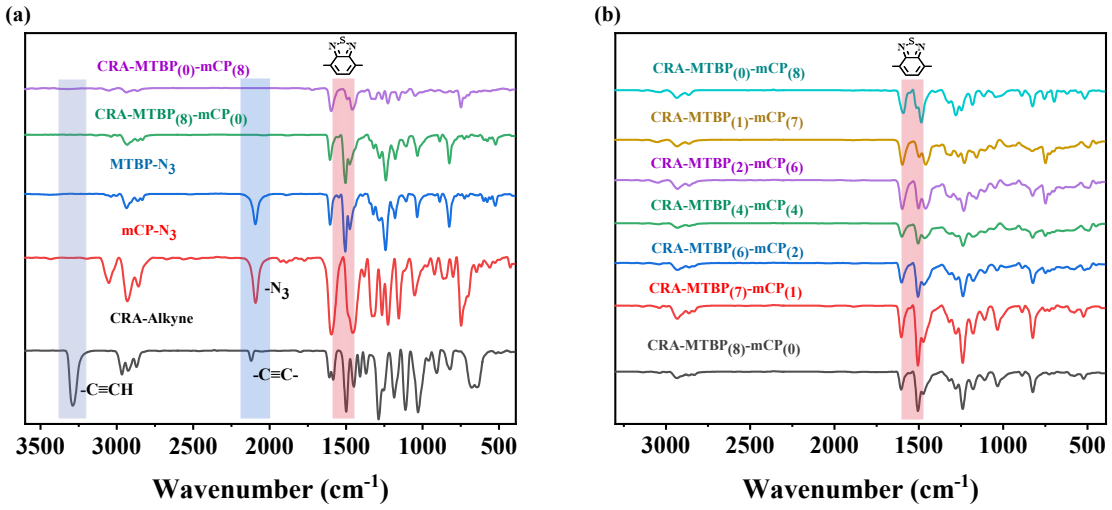

Fig. S4. FT-IR spectra of (a) CRA-MTBP$_{0)}$-mCP$_{(8)}$, CRA-MTBP$_{(8)}$-mCP$_{(0)}$, CRA-Alkyne, MTBP-N_3, and mCP-N_3; (b) CRA-MTBP$_{(X)}$-mCP$_{(8-X)}$ (X=8, 7, 6, 4, 2, 1 or 0).

6 Thermal analysis

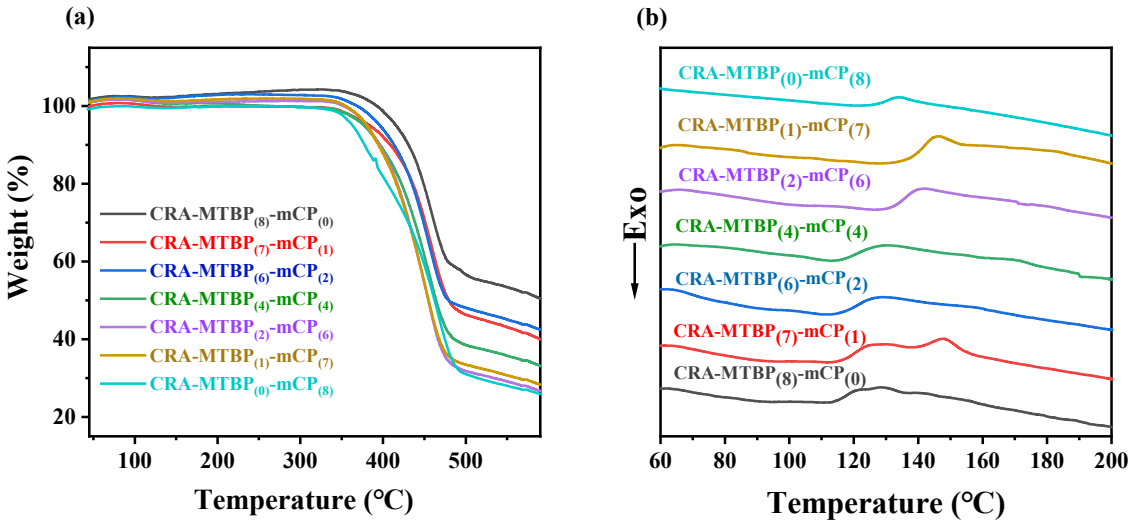

Fig. S5. (a) TGA curves and (b) DSC curves of CRA-MTBP$_{(X)}$-mCP$_{(8-X)}$ (X=8, 7, 6, 4, 2, 1 or 0).

7 XRD patterns

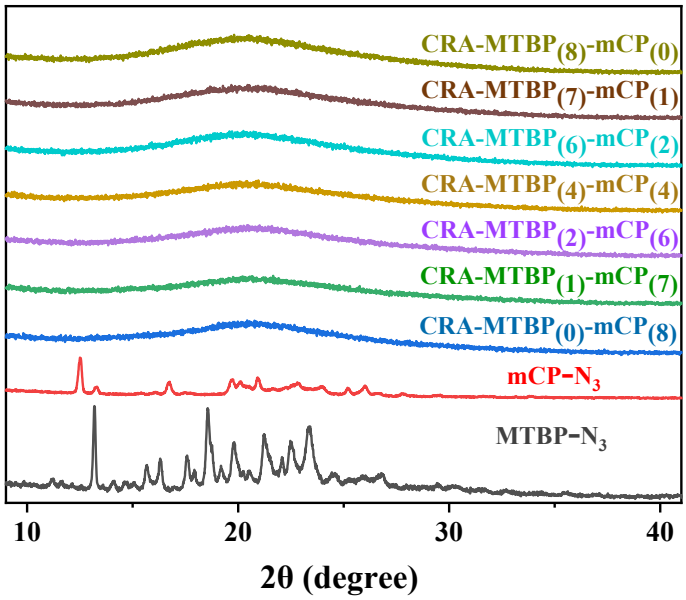

Fig. S6. XRD patterns of MTBP-N_3, mCP-N_3 and CRA-MTBP$_{(X)}$-mCP$_{(8-X)}$ (X=8, 7, 6, 4, 2, 1 or 0).

8 Cyclic voltammogram curves

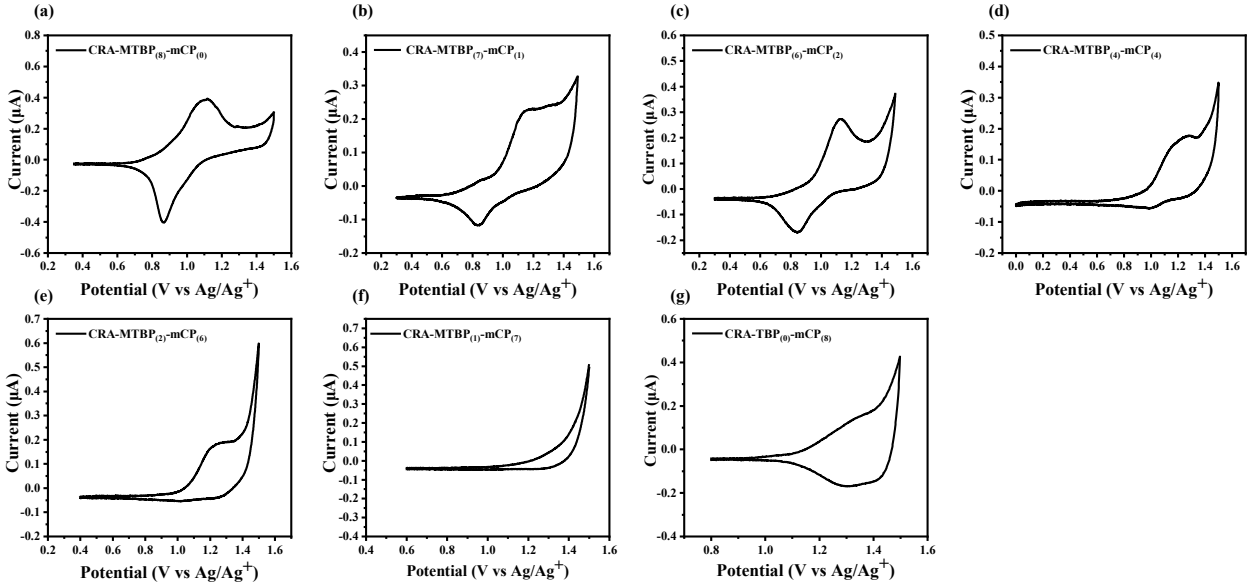

Fig. S7. Cyclic voltammograms of (a) CRA-MTBP$_{(8)}$-mCP$_{(0)}$; (b) CRA-MTBP$_{(7)}$-mCP$_{(1)}$; (c) CRA-MTBP$_{(6)}$-mCP$_{(2)}$; (d) CRA-MTBP$_{(4)}$-mCP$_{(4)}$; (e) CRA-MTBP$_{(2)}$-mCP$_{(6)}$; (f) CRA-MTBP$_{(1)}$-mCP$_{(7)}$; (g)CRA-MTBP$_{(0)}$-mCP$_{(8)}$.

9 Solvatochromic effect and supplementary photophysical properties

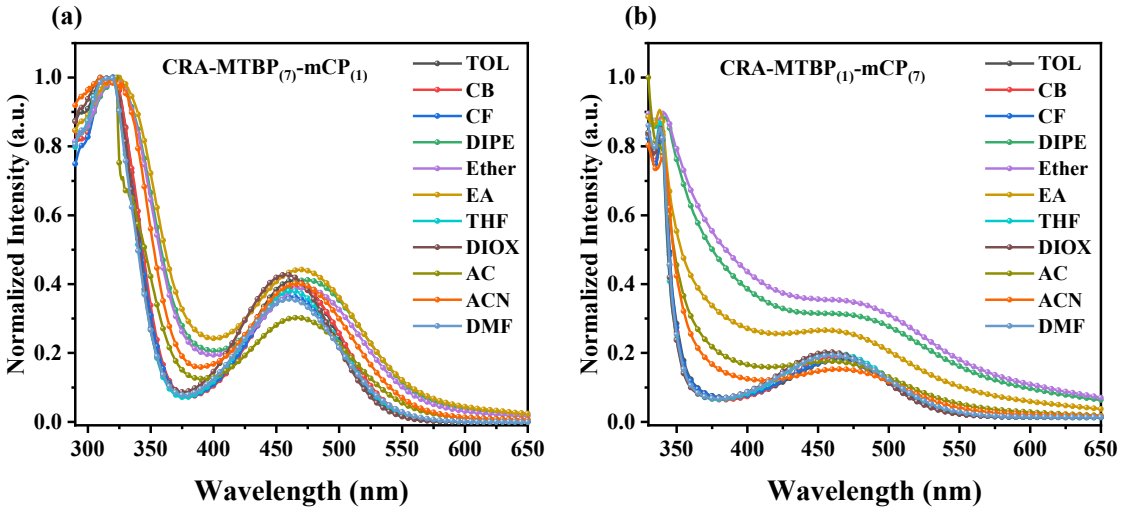

Fig. S8. UV-Vis absorption spectra of (a) CRA-MTBP$_{(7)}$-mCP$_{(1)}$ and (b) CRA-MTBP$_{(1)}$-mCP$_{(7)}$ in different solvents.

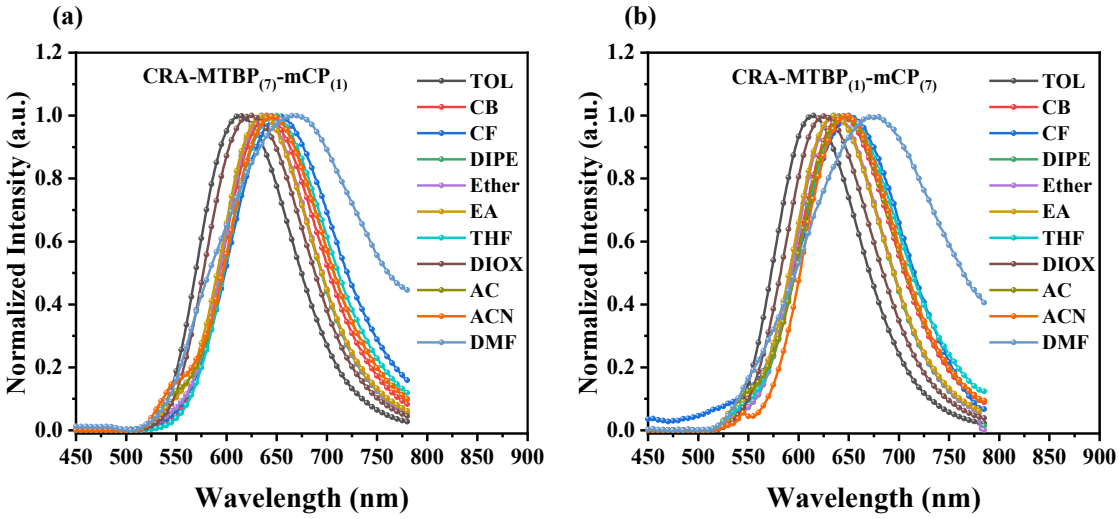

Fig. S9. PL spectra of (a) CRA-MTBP$_{(7)}$-mCP$_{(1)}$ and (b) CRA-MTBP$_{(1)}$-mCP$_{(7)}$ in different solvents.

10 Lippert−Mataga calculation

The effect of solvent polarity on the photophysical properties of CRA-TBP$_{(X)}$-mCP$_{(8-X)}$ (X=1 or 7) and CRA-MTBP$_{(X)}$-mCP$_{(8-X)}$ (X=1 or 7) was analyzed by using the Lippert-Mataga equation describing the interaction of the solvent with the dipole moment of the solute.

$$hc(v_a\text{-}v_f)=hc(v_a^0\text{-}v_f^0)-\frac{2(\mu_e\text{-}\mu_g)^3}{a^3}f(\varepsilon, n)$$

where f is the orientational polarizability of the solvent; $\upsilon_a{}^0$-$\upsilon_f{}^0$ corresponds to the Stokes shifts when f is zero; μ_e is the excited-state dipole moment; μ_g is the ground-state dipole moment; a is the solvent cavity (Onsager) radius, derived from the Avogadro number (N), molecular weight (M), and density (d = 1.0 g/cm^3); ε and n are the solvent dielectric and the solvent refractive index, respectively; and $f(\varepsilon,n)$ and a can be calculated, respectively, as follows.

$$f(\varepsilon, n)=\frac{\varepsilon\text{-}1}{2\varepsilon+1}\text{-}\frac{n^2\text{-}1}{2n^2+1}$$

$$a=(3M/4N\pi d)^{1/3}$$

Table S2 Solvatochromic UV-PL data for Lippert-Mataga model of CRA-MTBP$_{(X)}$-mCP$_{(8-X)}$ (X=1 or 7).

Solvents	Δf	CRA-MTBP$_{(1)}$-mCP$_{(7)}$			CRA-MTBP$_{(7)}$-mCP$_{(1)}$		
		λ_a (nm)	λ_f (nm)	υ_a-υ_f (cm^{-1})	λ_a (nm)	λ_f (nm)	υ_a-υ_f (cm^{-1})
TOL	0.014	455	617	5771	457	617	5674
CB	0.143	463	640	5973	465	641	5905
CF	0.149	462	641	6044	463	642	6022

Continue table S2 Solvatochromic UV-PL data for Lippert-Mataga model of CRA-MTBP$_{(X)}$-mCP$_{(8-X)}$ (X=1 or 7).

Solvents	Δf	CRA-MTBP$_{(1)}$-mCP$_{(7)}$			CRA-MTBP$_{(7)}$-mCP$_{(1)}$		
		λ_a (nm)	λ_f (nm)	υ_a-υ_f (cm^{-1})	λ_a (nm)	λ_f (nm)	υ_a-υ_f (cm^{-1})
DIPE	0.145	467	643	5861	469	645	5818
Ether	0.166	462	640	6020	463	642	6022
EA	0.200	459	640	6161	463	641	5998
THF	0.210	461	645	6188	462	647	6189
DIOX	0.021	460	622	5662	459	623	5735
AC	0.284	458	647	6378	461	648	6260
ACN	0.307	463	646	6118	464	649	6143
DMF	0.276	462	661	6516	463	660	6447

Δf is the orientational polarizability of the solvent; λ_a is the maximum absorption wavelength corresponding to intramolecular charge transfer (ICT) measured in different solutions; λ_f is the maximum emission wavelength measured in different solutions; υ_a-υ_f is the Stokes shifts.

11 Device fabrication and measurement

The OLED device structure was glass/ITO/PEDOT: PSS (40 nm) /PVK: poly-TPD (4/1, m/m) (30 nm) /EML (30 nm) /TmPyPB (40 nm) /CsF (1.2 nm)/Al (50 nm). The specific energy level alignments and molecular structures of organic compounds used in devices are shown in Fig. S10.

The manufacturing steps are as follows. Indium-tin oxide (ITO)-coated glass substrates were cleaned sequentially by deionized water, acetone and ethanol for 30 minutes each. After the UV-ozone treatment for 20 minutes, PEDOT: PSS was spin-coated onto the ITO substrate to give a 40 nm thick layer, followed by annealing for 5 minutes to stabilize the PEDOT: PSS layer. PVK: poly-TPD (4/1, m/m) was spin-coated onto PEDOT: PSS layer from chlorobenzene and annealed at 125 ℃ for 15 minutes to serve as a hole transporting layer. 30 nm of CRA-MTBP$_{(x)}$-mCP$_{(8-x)}$, which was used as the emitting layer, was spin-coated onto the PVK: poly-TPD layer from chlorobenzene and dried in the glovebox at 100 ℃ for 10 minutes. The electron transport layer (ETL) of TmPyPB (40 nm), the CsF (1.2 nm) dielectric layer and the Al (50 nm) metal layer were deposited in a vacuum, under a pressure of 8×10^{-5} Pa. The evaporation rates for the material deposition were 1-2 Å/s for TmPyPB, 0.1 Å/s for CsF and 10 Å/s for Al. The device's active area is about 0.1 cm^{-2}. The XPOY-EOE-350-1100 instrument was used to measure the current density, luminance, and driving voltage characteristics, as well as record the EL spectrum and EQE. All device tests were conducted inside a nitrogen-filled glovebox at room temperature.

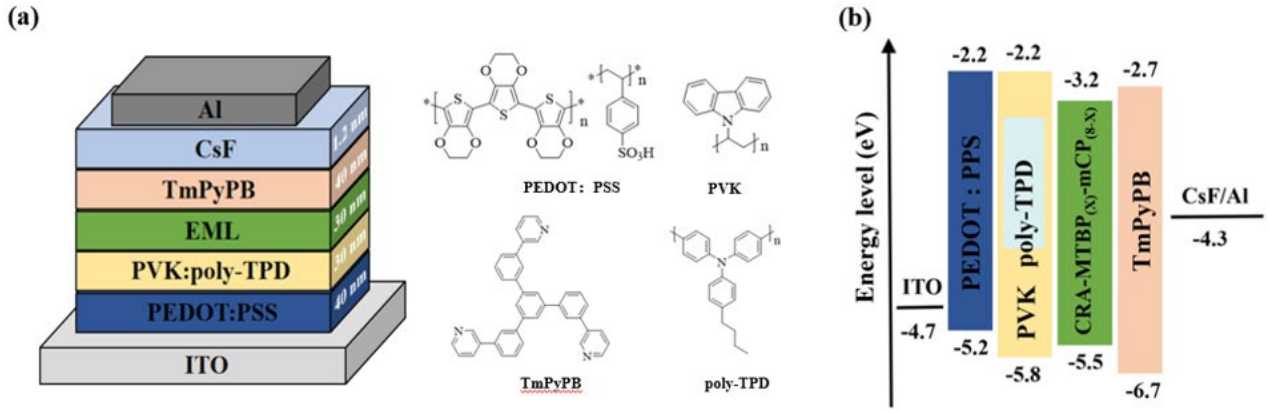

Fig. S10. (a) The device structure and chemical structures of organic compounds and polymers used; (b) The energy level alignments of CRA-MTBP$_{(X)}$-mCP$_{(8-X)}$.

12 OLED performance

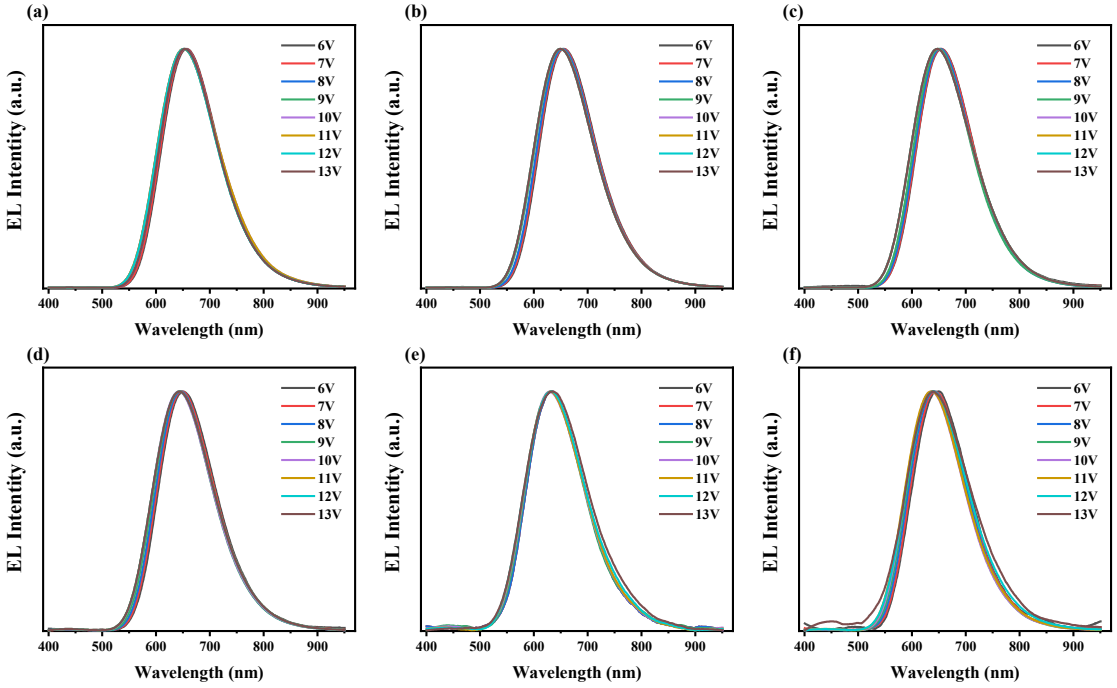

Fig. S11. EL spectra of (a) M1; (b) M2; (c) M3; (d) M4; (e) M5 and (f) M6 at different applied voltages.

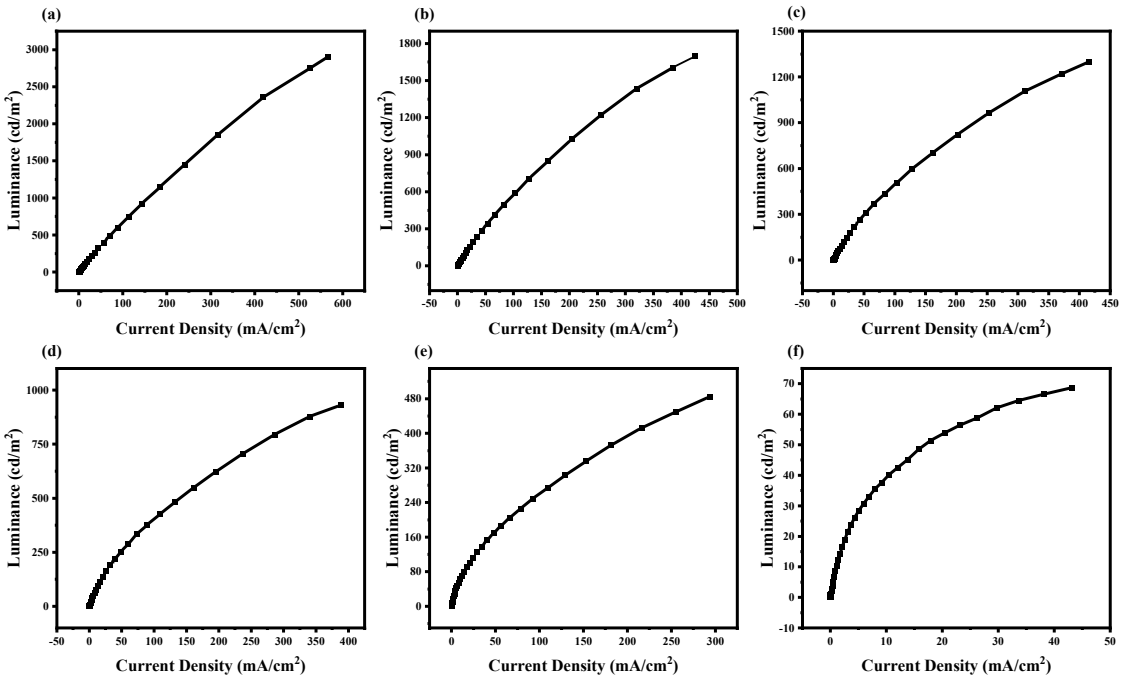

Fig. S12. The luminance-current density (L-J) characteristics of (a) M1; (b) M2; (c) M3; (d) M4; (e) M5 and (f) M6.

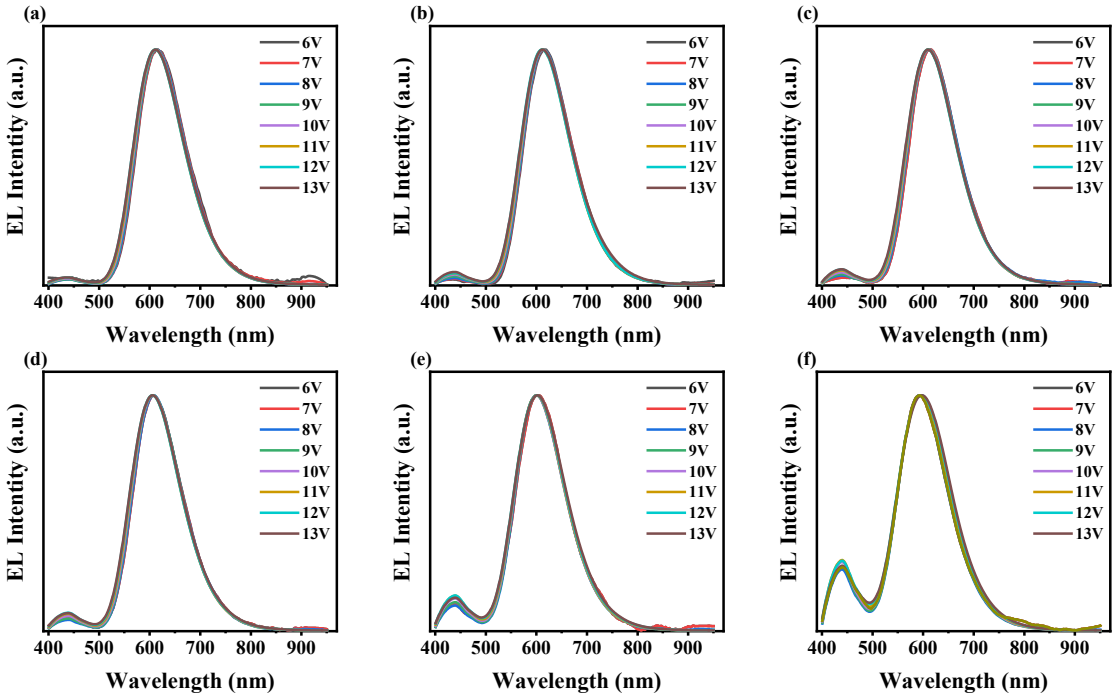

Fig. S13. EL spectra of (a) MD1; (b) MD2; (c) MD3; (d) MD4; (e) MD5 and (f) MD6 at different applied voltages.

13 Reference

[1] Wang FF, Qiu WD, Zeng J, Yuan P, Zong WS, Wu WB, et al. Calix [4] resorcinarene-based hyper-structured molecular thermally activated delayed fluorescence yellow-green emitters for non-doped OLEDs. J Mater Chem C.

2020; 8(13): 4469-4476.
[2] Zeng WX, Lai HY, Lee WK, Jiao M, Shiu YJ, Zhong C, et al. Achieving nearly 30% external quantum efficiency for orange-red organic light emitting diodes by employing thermally activated delayed fluorescence emitters composed of 1,8-naphthalimide-acridine hybrids. Adv Mater. 2018; 30(5): 1704961.
[3] Sun K, Y., Sun YB, Tian WW, Liu D, Feng YL, Sun YM, et al. Thermally activated delayed fluorescence dendrimers with exciplex-forming dendrons for low-voltage-driving and power-efficient solution-processed OLEDs. J Mater Chem C. 2018; 6(1): 43-9.
[4] Chen Q, Han BH. Prepolymerization and postpolymerization functionalization approaches to fluorescent conjugated carbazole-based glycopolymers via “click chemistry”. J Polym Sci, Part A: Polym Chem. 2009; 47(11): 2948-57.